CHEMISTRY OF MATERIALS

pubs.acs.org/cm

Article

Simple Synthesis, Structural and Electronic Characterization of Soluble Contorted Pentacenes

Karl J. Thorley,* Gehan S. Rupasinghe, Sashen Ruhunage, Moses Ogbaje, Vinayak Bhat, Sean Parkin, Chad Risko, Alexandra Paterson, and John E. Anthony

Cite This: https://doi.org/10.1021/acs.chemmater.6c00263

Read Online

ACCESS | Metrics & More | Article Recommendations | Supporting Information

ABSTRACT: Silylethynyl pentacenes have been a workhorse of small-molecule organic semiconductor research over the last two decades, but previous studies have identified dynamic disorder as a serious downfall for these materials. Thermal motion causing molecular vibrations results in fluctuation of the transfer integral between adjacent molecules and disrupts the charge transfer pathway through the bulk solid. In this work, we install phenyl damper groups onto the pentacene core of TIPS-pentacene to limit these vibrations, as observed by molecular dynamics simulations. Transistor devices show good hole mobilities and a consistent performance across a range of device dimensions. The damper groups also introduce a twist to the pentacene core, making these materials among a handful of contorted acene materials that still allow for π-stacking interactions applicable to electronics applications.

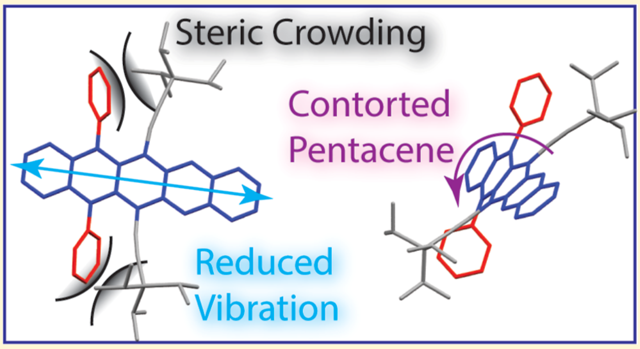

INTRODUCTION

Triisopropylsilylethynyl pentacene (TIPS-PN) has been a mainstay in organic electronics since its inception in 2001.[1] Real-world applications benefit from the increased solubility, processability, and stability of TIPS-PN compared with the parent unfunctionalized pentacene. The main application for TIPS-PN is in organic thin film transistors, with silylethynyl groups enabling deposition from solution processing techniques. The size and shape of the alkyl chains on the silyl groups are a driving force for the optimal arrangement of the electronically active pentacene cores into motifs suitable for charge transport.[2] The two-dimensional (2D) brickwork packing of TIPS-PN offers multiple directions for charge transport through the solid,[3] while the layered structure influences crystal growth during deposition, allowing larger crystalline domains and fewer boundaries, which can influence charge mobility.

One problem identified in small-molecule organic semiconductors such as TIPS-PN is the variation of molecular alignment due to thermal motions.[4] Even small relative displacements between a pair of molecules can drastically influence the transfer integral (or electronic coupling) between them,[5] which ultimately affects charge transport based on the hopping mechanism proposed by Marcus theory. The charge transfer integral, *t*, is dependent on the spatial overlap of molecular orbitals on adjacent molecules and therefore on the spatial distribution of these orbitals within the molecule. This means that even when a pair of molecules have large area overlap, charge transport may be limited by the regions of low orbital overlap (e.g., due to the location of nodes in the wave function). Even small movements such as those by translation or rotation of a molecule by thermal energy are enough to cause a distribution of transfer integrals, which affects the ability of the solid to act as a semiconductor.[6]

For TIPS-PN, the so-called "killer phonon" mode is described as the pentacene long-axis translation,[7] a motion allowed due to the flexibility of the C−C triple bond (Figure 1). In the solid-state, the bulky silyl groups are locked in place in the crystal lattice, and the bending motion of the alkyne results in a translational motion of the pentacene cores. This translational mode has the highest impact on variability of the transfer integral, as it results in variations of overlap of nodes and/or lobes of the molecular orbitals.[7] In this work, substituents are introduced onto the pentacene adjacent to the flexible alkyne groups to dampen this oscillation, with the goal to improve the consistency of the charge transfer pathways through the solid state. Beyond cata-functionalization to affect electronic properties,[8] core functionalization of TIPS-PN at the peri-positions is surprisingly under-reported.[9]

Received: January 27, 2026
Revised: March 17, 2026
Accepted: March 23, 2026

© XXXX The Authors. Published by American Chemical Society

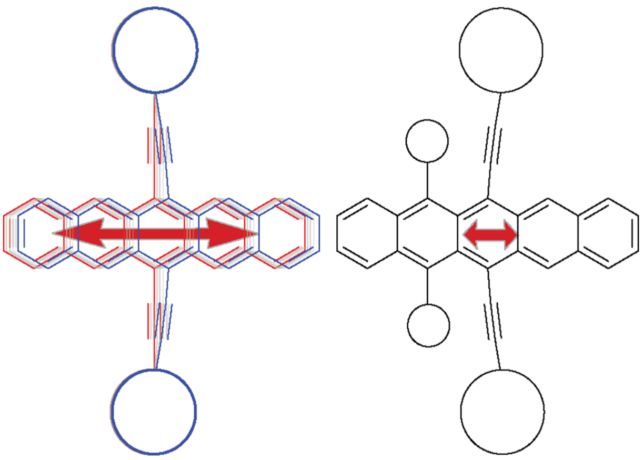

Figure 1. Dampening molecular oscillation by chemical functionalization adjacent to the flexible alkyne triple bond.

1,4,8,11-tetramethyl-TIPS-PN is the only peri-derivative to have been explored as a part of a study on dynamic disorder, and the effect of these outer-ring substituents was found to be minor[7] despite their high hole mobilities.[10] Our current strategy places the substituent directly next to the alkyne, whose flexibility is a source of the solid-state thermal disorder. Restricting the bending mode of the alkyne by this direct steric encumbrance should have a stronger effect on solid-state vibration than more remote end-ring functionalization.

In a bid to rigidify the alkynyl bond of TIPS-PN, we investigated the installation of functional groups at the adjacent benzenoid ring, opting to introduce phenyl rings to form materials reminiscent of the sterically crowded tetracenes reported by Thomas et al.[11] Those tetracenes featured a backbone twist angle of 31° but showed no π-stacking in the solid-state due to the larger volume of side groups on the molecular periphery. The use of phenyl groups is also reminiscent of the high mobility tetracene derivative, rubrene, which adopts a twisted structure in gas-phase simulations but becomes planarized in its characteristic herringbone crystal packing motif.[12] Derivatives of rubrene substituted on the phenyl rings typically retain the twisted single-molecule geometry of the parent molecule and adopt one of two solid-state structural motifs; either they adopt the herringbone packing with planarization of the tetracene core[13] or they retain a twisted core but exhibit no backbone stacking.[14] In only very few cases, the partial substitution of the phenyl rings of rubrene results in a contorted tetracene that exhibits backbone stacking in its crystal structure.[12,15]

Other contorted acene-containing molecules have been reported[16] or explored computationally,[17] although the large increase in side-chain volume required to induce the geometric distortion again precludes these materials from use as semiconductors. The only example of a core-contorted pentacene derivative[18] includes phenylene bridging groups that eliminate the possibility of acene backbone stacking. Initial density functional theory (DFT) geometry optimizations of phenyl-functionalized TIPS-PN (referred to from here-on as TIPS-PhPN, Scheme 1) suggest a twisted core of around 30° but with an accessible π-surface for organic electronics applications relying on intermolecular interactions for charge transport.

RESULTS AND DISCUSSION

Synthesis

In keeping with our desire to employ simple, transition-metal-free, and sustainable approaches to organic semiconductor preparation, the synthesis of TIPS-PhPN starts with the naturally occurring quinone Quinizarin **1** (Scheme 1). Addition of phenyllithium to the center-most carbonyl groups followed by tautomerization under acidic conditions furnished the diphenyl 1,4-anthraquinone **2** in acceptable yield on multigram scale. Reduction with sodium dithionite gave the hydroquinone **3**, which was assumed to possess limited oxidative stability and reacted without haste under aldol conditions with phthalaldehyde to yield the diphenyl pentacene quinone **4**. The introduction of phenyl groups gave the quinone sufficient solubility to purify by chromatography on silica. Addition of trialkylsilyl acetylide and deoxygenation with tin(II) chloride under standard protocols yielded the target phenyl-functionalized pentacenes in good yields. The synthesis is highly adaptable, allowing the installation of different damper groups and different alkynyl groups to different acene cores. We report here on our initial

Scheme 1. Synthesis of Diphenyl Silylethynyl Pentacenes (TIPS-PhPN and TES-PhPN)

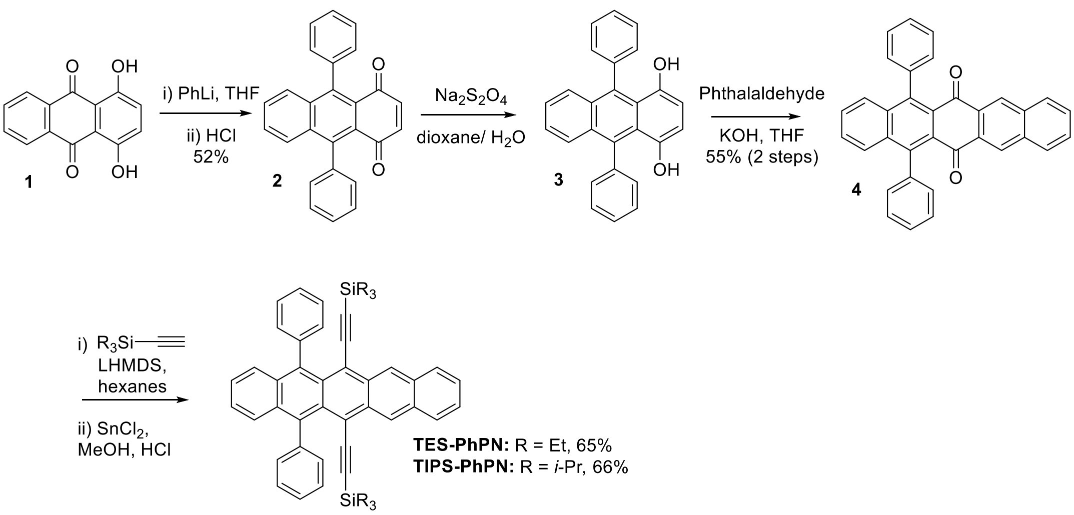

two derivatives of diphenyl pentacenes, TES-PhPN and TIPS-PhPN.

UV/Vis Spectroscopy

From absorption spectroscopy (Figure 2), TIPS-PhPN showed a red shift versus TIPS-PN likely due to the electronic induction effects of the additional phenyl groups and a broadening of the entire visible absorption bands likely due to the induced core twisting of the pentacene framework. Density functional theory (DFT, IP-tuned ωB97XD/6-31G*) calculations reveal a core pentacene twist of around 30°. Changing the size of the trialkylsilyl groups from TES to TIPS results in minor modifications to twist angles and ethynyl bending, which manifest as small shifts in the solution absorption spectra. Surprisingly, the molecules were practically non-emissive in solution (Figure 2). This is in stark contrast with the crowded tetracenes synthesized by Thomas where fluorescence quantum yields of 75% were reported.[11]

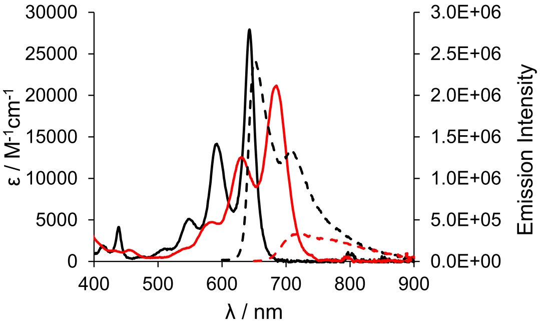

Figure 2. UV−vis extinction coefficient (solid lines) and fluorescence (dashed lines) spectra of TIPS-PN (black) and TIPS-PhPN (red) measured in chloroform at 293 K. Fluorescence spectra from samples of similar absorbance at the excitation wavelength.

Electrochemical analysis shows a shift in the oxidation potential of +0.15 V for TIPS-PhPN compared to that for TIPS-PN, while the reduction peak is shifted by +0.05 V (Figure S11). This results from the HOMO of TIPS-PhPN being raised in energy versus TIPS-PN while the LUMO is raised only slightly, resulting in a smaller HOMO−LUMO gap and thus red-shifted optical absorption. Houk and Norton predicted a narrowing of the HOMO−LUMO gap with increasing core twist for the acene family.[17] These trends are supported by DFT results (IP-tuned ωB97XD/6-31G*) where TIPS-PhPN has an ionization potential 0.15 eV smaller than that of TIPS-PN, while the electron affinities of both molecules are close to identical (Table S6). Neither HOMO nor LUMO distribution is observed on the phenyl rings through partial density of states DFT calculations at the same level of theory, suggesting that changes in these MO energies come from inductive effects of these groups and the induced core twists. Time-dependent DFT calculations show that the lowest energy excitations are purely HOMO-to-LUMO in character for both TIPS-PN and TIPS-PhPN, and that this excitation energy is 0.1 eV smaller in TIPS-PhPN. UV−vis measurements under constant white light irradiation also revealed an increased photostability of TIPS-PhPN versus the parent TIPS-PN (Figure S12). A more thorough investigation into single-molecule optoelectronic properties of these materials is underway.

Vibrational Spectroscopy

Fourier transform infrared (FTIR) spectroscopy was used to analyze differences in molecular vibrations upon the inclusion of the phenyl rings (Figure 3). This experimental data was supported by DFT frequency calculations, using B3LYP/6-31G* to reoptimize the molecular geometry and frequency analysis with an established scaling factor[19] for vibrational frequencies. Of note in the FTIR spectra are the alkyne stretches around 2100 cm^{-1}, which are reproduced well by the DFT calculations. The higher energy asymmetric stretch of the two alkynes is shifted by −10 cm^{-1} in TIPS-PhPN, while the slightly lower energy symmetrical stretch is more intense in the experimental spectrum of TIPS-PhPN due to the lower symmetry of the molecule. A peak is observed at 800 cm^{-1} in TIPS-PhPN that is completely absent in TIPS-PN, resulting from a combination of alkynyl vibrations and the movement of the adjacent phenyl rings. Other notable differences are observed in the fingerprint region, including additional peaks at 760, 700, and 560 cm^{-1} in TIPS-PhPN that are not present for TIPS-PN, and shifts in other signals such as at 1370 cm^{-1} arising from pentacene ring vibrations effected by the attachment of the phenyl rings and desymmetrization of the molecule. The vibrational modes responsible for all mentioned IR absorbances are depicted in Figure S16. Unfortunately, FTIR spectroscopy does not provide information on the lowest energy intermolecular modes that are most responsible for the transfer integral variation. Nonetheless, the differences in the observable IR absorbances hint at the role of the additional phenyl groups in affecting molecular vibrations.

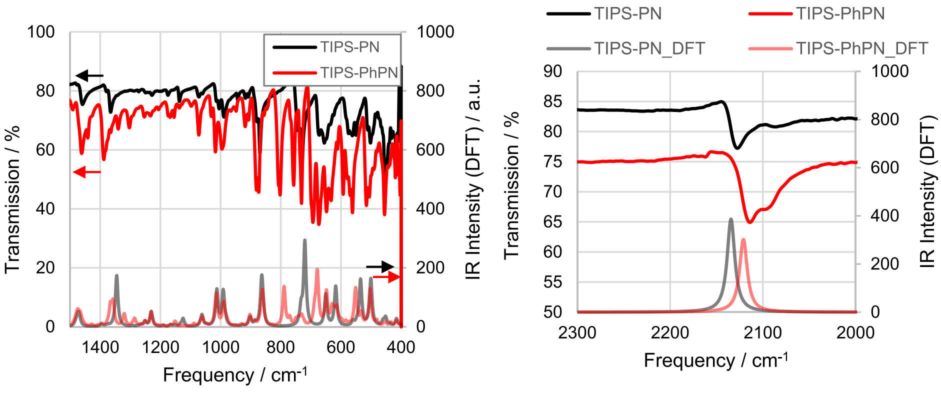

Figure 3. Experimental (top, measured on microcrystalline powders) and computed (bottom, scaled B3LYP/6-31G*) IR vibrational spectra of TIPS-PN (black) and TIPS-PhPN (red).

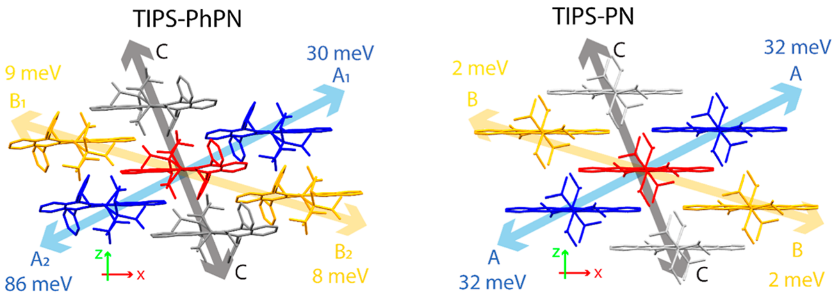

Figure 4. Packing motif of single layers of TIPS-PhPN and TIPS-PN molecules from single-crystal X-ray diffraction, indicating definitions of molecular stacking directions used in the main text. Transfer integrals (PBE0/6-31G*) computed from molecular pairs extracted from the crystal structure provided in meV.

Crystal Packing

Of prime importance to the use of these materials as organic semiconductors is their crystal packing, such that charges can migrate through the bulk material according to the overlap of adjacent pentacene π-systems. While TIPS-PN crystallizes readily from hot acetone solutions, TIPS-PhPN and TES-PhPN derivatives had limited solubility under similar conditions, resulting in poor crystal growth. Instead, single crystals suitable for X-ray analysis were grown for each of the TES- and TIPS-PhPN by slow cooling of saturated butanone solutions. Both crystal structures featured twisted pentacene cores, with dihedral angles around 25° between the terminal rings, similar to the sterically crowded tetracenes of Thomas and co-workers.[11] In contrast to those tetracenes or the variety of other twisted acenes that do not exhibit any π-stacking interactions, increasing the length of the acene core allowed such face-to-face interactions to occur, making these pentacenes suitable for solid-state charge transport applications.

Previously established design rules associated the ratio of the solubilizing groups and the acene core with the type of observed packing motifs in single crystals. With the addition of the phenyl groups, one might predict that the slightly smaller triethylsilyl groups would yield a combined solubilizing group comparable to a TIPS group and thus the desirable 2D brickwork packing exhibited by TIPS-PN. X-ray analysis (Figure S13) revealed that TES-PhPN adopts a 1D slip-stack configuration that is similar to the related TES-PN.[2] A staircase of backbone stacking interactions provides a pathway for charge transport through the material in a single direction, but transport in other directions is disrupted due to the interdigitation of TES and Ph side chains with π-faces of adjacent pentacene stacks.

The packing of TIPS-PhPN in single crystals is broadly similar to that of TIPS-PN despite the increase in side-chain volume. Figure 4 shows molecular interactions in three different directions within single stacks of this packing motif arranged around a central molecule highlighted in red. A roughly 2D brickwork pattern is observed where π-stacking interactions are present on both faces in the *A*-direction. These alternate between two phenyl substituted ends interacting (A_1), followed by two unsubstituted ends of the pentacenes interacting (A_2). In the *B*-direction of Figure 4, one of the molecules forms a π-stacking interaction (B_1), but the other molecule is offset along the pentacene short axis direction such that there is no overlap of the pentacene surfaces (B_2). The final intrastack interaction in the *C*-direction does not have direct $\pi-\pi$ overlap with the central red molecule since the other A and B pentacene molecules are sandwiched in between, but interactions in the C molecular pairs between the side chains can aid stabilization of the solid-state structure. The interactions above and below the central molecule are identical in this direction. The crystal packing of TIPS-PN can be described by these same directional descriptors, except that the interactions in each direction are symmetrical (i.e., $A_1 = A_2$ and $B_1 = B_2$).

In general, the center-of-mass distances between pentacene cores are increased in TIPS-PhPN versus TIPS-PN due to the extra side-chain volume (Tables S4 and S5) by over 1 Å in each molecular pair and particularly in the pentacene long-axis direction (e.g., an increase from 6.7 to 8 Å for the closest packed pairs). The distances in the π-stacking direction of TIPS-PhPN are surprisingly small when considering the center-of-mass displacements (e.g., 3.1 Å, Table S5), but due to the twisted nature of the TIPS-PhPN core, a more representative π-stacking distance is derived from the plane-to-plane distance of overlapping rings only. These π-stacking distances are comparable to those in TIPS-PN (3.3 to 3.6 Å), with a smaller distance for the offset molecular pair B_2 where no π-stacking occurs.

Electronic communication between adjacent molecules in the crystals was assessed using DFT calculations, using PBE0 functional[20] lacking Hartree−Fock exchange that can inflate the coupling values.[21] Despite the increased spacing, computed transfer integrals using molecular dimers extracted from the X-ray crystal structure of TIPS-PhPN are in fact higher (up to 86 meV) than those in TIPS-PN (up to 32 meV). The transfer integrals in TIPS-PhPN are anisotropic, with much larger coupling in the *A*-direction, while the other π-stacking *B*-direction has $t_H < 10$ meV. Within the main charge transport *A*-direction, there is further asymmetry due to the substitution pattern of the pentacene; the A_1 pair where the phenyl groups interact with each other has $t_H = 30$ meV, while the greater backbone overlap of the unsubstituted ends of the pentacenes in pair A_2 yields $t_H = 86$ meV. Similar asymmetry is observed in the 1D slipped stack of TES-PhPN, where transfer integrals of 27 and 63 meV are determined.

As well as the volume of the side chains, the electronic nature of solubilizing groups affects the intermolecular noncovalent interactions between adjacent molecules and thus the preferred packing arrangement in the crystal.[22] Symmetry adapted perturbation theory (SAPT0/jun-cc-pvdz)[23] interaction energies between molecular pairs extracted from X-ray structures are shown in Figure 5, plotted against the center-of-mass displacement between pentacene cores. Energy decomposition analysis of these interactions is provided in

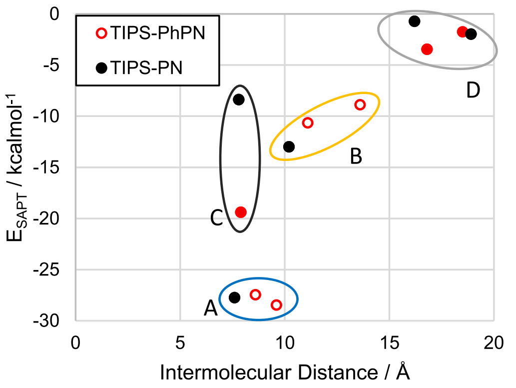

Contact C	ES	EX	DISP	IND
TIPS-PN	-0.6	3.4	-10.8	-0.4
TIPS-PhPN	-4.4	11.4	-25.0	-1.4

Figure 5. SAPT computed interaction energies versus molecular displacement for pairs of molecules from the TIPS-PN (black) and TIPS-PhPN (red) X-ray crystal structures. Data points are grouped according to similar interacting pairs within the packing motif, where duplicate interactions are shown as filled circles and single interactions as open circles. SAPT decomposition energies for contact C are presented in table in kcal/mol (ES = electrostatic, EX = exchange, DISP = dispersion, and IND = induction).

Figures S20 and S21. For the symmetrical TIPS-PN, each of these interactions is duplicated in the crystal, shown as filled black circles. The symmetry breaking of TIPS-PhPN molecular structure results in nonequal interactions of similar type (A_1 vs A_2, etc.) giving two open circles a shown in Figure 5. The *C*-interactions are identical, and so this interaction is shown as a duplicate data point with filled circles. In all molecular pairs, the dominant intermolecular forces from energy decomposition are attractive dispersion and repulsive exchange interactions with much smaller contributions from electrostatics and induction effects. The strongest interacting pair in TIPS-PN with a separation of 7.6 Å (group A, Figure 5) becomes split into two separate interactions in TIPS-PhPN due to asymmetry, with slightly increased molecular spacing not significantly affecting the binding energies. The backbone stacking in the opposite diagonal direction (group B, Figure 5) is composed of molecular pairs with slightly increased displacement and weaker binding by around 2 kcal/mol compared to the same interactions in TIPS-PN. The increase in distance reduces both the stabilizing dispersion interaction and the destabilizing exchange interaction, the net outcome being a smaller binding energy between the two molecules. The final intrastack interaction (group C), made up from the central pentacene with another molecule two layers vertically above, is vastly different between TIPS-PN and TIPS-PhPN, where the interaction is twice as strong for the same molecular displacement in TIPS-PhPN. This interaction does not involve any backbone overlap, since there is another layer of pentacenes between the two interacting pairs. Instead, the interaction is made only of side chains (TIPS and Ph groups), and the increased size in TIPS-PhPN results in greater dispersion stabilization, outweighing any negative effects of increased steric repulsion (exchange energy). The group C interaction and the importance of side-chain interactions are already shown to be important to stabilization of in silico theoretical polymorphs of TES-PN and TIPS-PN.[22] Further interactions between stacks (group D) are small and at larger molecular distances but offer some slight stabilization of the crystal packing motif. Overall, the noncovalent interactions between adjacent TIPS-PhPN molecules in the crystalline environment retain similar (or even increased) binding energies as TIPS-PN despite the increased side-chain size, leading to the adoption of a brickwork-like packing.

Molecular Motion and Changes in the Transfer Integrals

To probe whether the molecule redesign of TIPS-PN to limit molecular motion was successful, we employed molecular dynamics (MD) simulations to probe the range of molecular movement within a 3 × 3 × 3 supercell, using the experimental crystal structures of TIPS-PN and TIPS-PhPN as starting points. After equilibration, 20 ns simulations were carried out at 293 K to analyze the effect of thermal energy, sampling 100 separate time frames from the simulations at 200 ps intervals for distance measurements and transfer integral calculation on four different molecular pairs (A_1, A_2, B_1, and B_2). Distances were measured directly in Gromacs software, while transfer

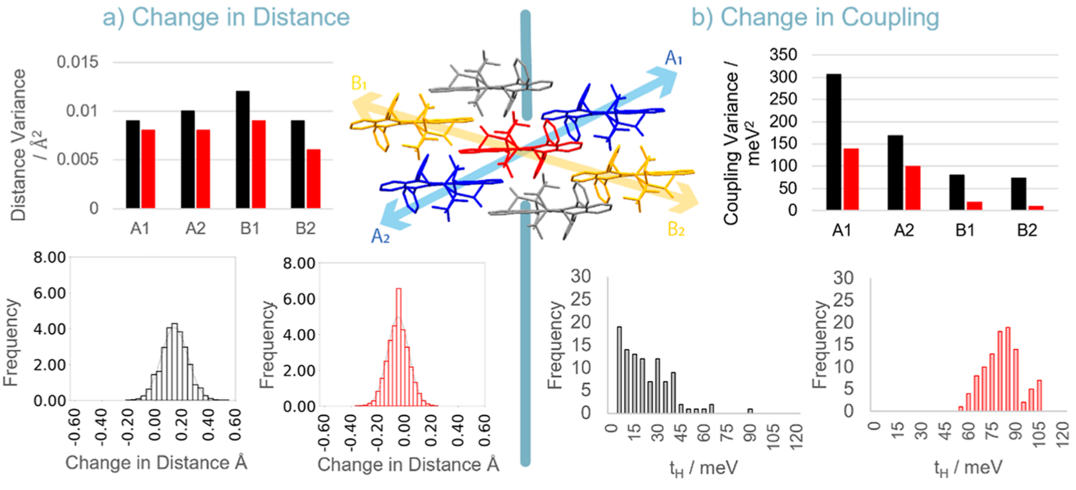

Figure 6. Distribution of (a) center-of-mass pentacene−pentacene distances and (b) electronic couplings for molecular pairs of TIPS-PN (black) and TIPS-PhPN (red) from MD simulations at 293 K. (Top) variance of distances or coupling for each π-stacked pair and (bottom) distributions of distances or coupling for pair A_2 at 200 ps intervals over 2 ns simulation.

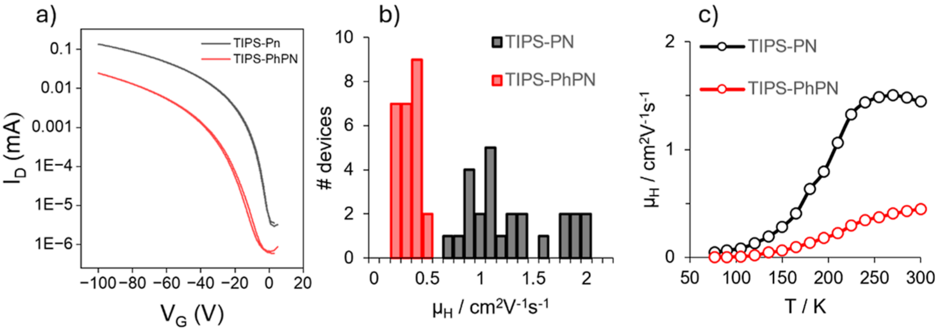

Figure 7. (a) Transfer curves of the best-performing TIPS-PN and TIPS-PhPN transistors (each as a 1:1 pentacene/PTAA blend). (b) Hole mobility measurement distribution across 24 transistor devices with varying channel dimensions. (c) Temperature dependence of the hole mobility of devices with channel length 80 μm. TIPS-PN = black and TIPS-PhPN = red.

integrals were calculated on extracted dimer geometries by using PBE0/6-31G*.

The five centermost molecules forming the 2D brickwork motif were used to assess the intermolecular interactions in the bulk of the crystal, with the four corner atoms of the pentacenes used to determine the dimensions of the pentacene cores. The distribution of the distances between the centers of these pentacene cores is shown in Figure 6a. All molecular pairs of TIPS-PhPN show smaller or comparable deviations in intermolecular distance when compared to TIPS-PN, for each of the molecular pairs within the crystal packing motif. For example, for the closest backbone-stacked pair A_1 visualized in Figure 6, the variance of TIPS-PhPN distances is 0.006 Å which increases to 0.009 Å in TIPS-PN. Variance of all pairs is shown top-left of Figure 6, while histogram distributions are provided as Supporting Information (Figure S18).

Transfer integrals were assessed by DFT calculations (PBE0/6-31G*) for the same centermost pentacene cluster of the MD simulations, as shown in Figure 6, using the same time samples and geometries extracted for distance measurements. The modest basis set[24] allowed for the calculation of 100 transfer integrals for each of the molecular pairs for both TIPS-PN and TIPS-PhPN, a total of 800 transfer integral calculations. The mean coupling values of these MD + DFT simulations differ from those calculated on the static crystal structure coordinates calculated at the same level of theory due to the slight molecular realignments and unit cell expansion during MD relaxation and increased temperature (Tables S7−S10). Furthermore, the coupling values of TIPS-PN are no longer fully symmetrical within each A/B direction due to fluctuations in molecular alignments, with limited sampling capturing only a fraction of all time steps available during the simulation. The molecular pairs with higher coupling in TIPS-PN decrease from $A_1 = A_2 = 32$ meV when calculated on the crystal structure to mean values of $A_1 = 19$ and $A_2 = 12$ meV. The similar couplings in TIPS-PhPN are $A_1 = 40$ and $A_2 = 79$ meV ($A_1 = 31$ and $A_2 = 89$ meV for X-ray determined pairs). This suggests that the TIPS-PhPN packing structure is less affected by the increasing temperature and expanding system size, as probed by the MD simulations.

The variance of the coupling values over time tells a similar story. For each molecular pair (A_1, etc.) in TIPS-PhPN, the coupling varies by a smaller amount than the equivalent pair in TIPS-PN (Figure 6b). It is also noticeable that the couplings in TIPS-PN pass through $t_H = 0$ as the molecular pairs lie close to the overlap of nodes in the respective HOMO on each molecule. This is also true for pairs B_1 and B_2 in TIPS-PhPN, but pairs A_1 and A_2 exhibit coupling that is always present, varying between 50 and 100 meV for A_1 for example. While TIPS-PN and TIPS-PhPN are not suitable n-type materials due to a high energy LUMO, the LUMO−LUMO transfer integrals (Figures S20 and S21) show similar trends in variance to the HOMO−HOMO interactions, highlighting that even changing the spatial distribution of the orbitals results in more consistent electronic communication in TIPS-PhPN due to the constrained molecular movement. This more consistent electronic coupling in TIPS-PhPN is promising for the applications relying on solid-state charge transfer, and the combination of smaller variation in molecular displacements and electronic couplings for TIPS-PhPN justifies our molecular design approach, which can continue to be refined with other derivatives in future studies.

Transistor Fabrication and Testing

To assess the impact of molecular phenyl substitution in TIPS-PhPN on charge transport in solid-state devices, top-gate bottom-contact organic thin film transistors were fabricated, and hole mobilities were measured in the saturation regime. Given the similarity in solid-state packing between TIPS-PhPN and TIPS-PN, the work here focused on comparing TIPS-PhPN with TIPS-PN, rather than comparing TIPS-PhPN with the 1D slip-stack TES-PhPN. The active layer thin films (i.e., the transistor channels) were formed as neat materials, as well as in blends where the small molecule was combined with poly[bis(4-phenyl)(2,6-trimethylphenyl)amine] (PTAA) at a 1:1 ratio. The latter blending technique influences how small molecules crystallize in the solid-state, and incorporating such semiconducting polymer binders with small-molecules has been shown to increase mobility by an order of magnitude compared to neat small-molecule films.[25] Similarly, the blend devices shown here showed the highest mobilities: TIPS-PN/PTAA 1:1 blend devices showed mobilities up to 2.0 cm^2 V^{-1} s^{-1}, with an impressive average mobility of 1.9 cm^2 V^{-1} s^{-1}, when taken from five devices at the best-performing channel length (100 μm) (Figure S30). Comparatively, neat TIPS-PN had a maximum mobility of 0.64 cm^2 V^{-1} s^{-1}, with an average of 0.50 cm^2 V^{-1} s^{-1} across five devices with the best-performing 100 μm channel length. On the other hand, TIPS-PhPN/PTAA 1:1 blend devices showed a highest mobility of 0.42 cm^2 V^{-1} s^{-1}, with an average mobility of 0.36 cm^2 V^{-1} s^{-1}, taken from five devices at the best-performing channel length (80 μm) (Figure S36); in contrast, maximum and average mobilities of neat TIPS-PhPN are an order of magnitude lower than the TIPS-PhPN/PTAA blend. The lower observed charge mobility in TIPS-PhPN might be due to a number of factors, including lower solubility of the material (noted in the single-crystal growth conditions earlier), which results in less ideal film growth and more grain boundaries in the film. Polarized optical microscopy suggests this is the case with larger crystalline domain sizes for TIPS-PN than TIPS-PhPN films (Figure S24). However, while the hole mobilities of the TIPS-PhPN blends are lower values than the TIPS-PN blends—when a broad range of channel lengths are considered (from 30 to 100 μm, Figure S36), the device-to-device variation is noticeably improved in the TIPS-PhPN blends, when compared to TIPS-PN blends. Namely, TIPS-PN blend mobilities vary from 0.11 to 0.42 $cm^2\ V^{-1}\ s^{-1}$, whereas TIPS-PN devices vary in mobility by over 1 $cm^2\ V^{-1}\ s^{-1}$ (Figure 7b). The latter indicates that TIPS-PhPN is more resilient to contact resistance effects, with enhanced uniformity and less overall impact from channel length variation.

Changes in vibrational freedom should become evident with changes in the thermal energy. Charge carrier mobility was therefore measured across a range of temperatures, from 77 to 300 K, for TIPS-PN blend and TIPS-PhPN blend devices with a fixed channel length (80 μm). Charge carrier mobilities decrease at lower temperature (Figure 7c), indicating that localized carriers dominate charge transport in both TIPS-PN and TIPS-PhPN systems, with hopping being the main transport mechanism. Here, hopping transport likely arises from defects in the crystals such as grain boundaries. While band-like transport has been observed for TIPS-PN, this observation required shallow trap-filling with high drain and gate voltages in short-channel devices.[26] The rate with which mobility decreases as the temperature is decreased is more pronounced for TIPS-PN than for TIPS-PhPN (Figure 7c). At higher temperatures, the mobility is higher because the carriers have more thermal energy to leave the trap states and contribute to transport.

For TIPS-PN, an initial small increase in mobility upon cooling from 300 K is observed, where a maximum mobility of 1.5 $cm^2\ V^{-1}\ s^{-1}$ is reached at 270 K. This supports a secondary thermal effect, which is consistent with thermal vibrational disorder of the TIPS-PN molecules. The drop in temperature provides less thermal energy for the molecules to vibrate, meaning more consistent intermolecular coupling that leads to slightly increased charge mobility. Over a wider temperature range between 230 and 300 K gradual changes in mobility for the TIPS-PN device are observed due to the trade-off of separate thermal effects—the reduced thermal disorder with decreasing temperature which increases mobility and the increasing number of trap states with decreasing temperature that decreases mobility. The trend in mobility vs temperature of the TIPS-PhPN device is much more consistent, suggesting a system that is less affected by these thermal motions.

CONCLUSIONS

We developed a simple, scalable synthesis of sterically crowded contorted pentacenes aimed at addressing the problem of dynamic disorder and transfer integral fluctuation in the OFET devices. Despite the increased steric bulk of the solubilizing groups, two derivatives (TES-PhPN and TIPS-PhPN) exhibit substantial backbone stacking interactions in the solid state, such that they are suitable for charge transport studies. We directly compared the TIPS-PhPN derivative to organic electronics stalwart TIPS-PN, which exhibits brickwork packing configurations similar to those in the solid state. MD simulations support a decrease in the magnitudes of intermolecular fluctuations, with more consistent transfer integrals being computed throughout the simulations for TIPS-PhPN. Transistor devices of TIPS-PhPN exhibit mobilities of 0.36 $cm^2\ V^{-1}\ s^{-1}$ which although lower than TIPS-PN are still reasonable despite the increased molecular spacing by the additional side groups. These devices show an almost constant increase in mobility with temperature, suggesting that the additional rigidification of the molecular structure influences the intermolecular interactions in the crystalline state, and the mobilities across a range of devices are more consistent for TIPS-PhPN than for TIPS-PN. The combination of steric clashing of side chains at the center of the molecule without hindering accessibility of the π-surface makes these materials among the first contorted acenes that can be utilized in organic electronics applications.

EXPERIMENTAL SECTION/METHODS

Synthesis and Characterization

General Information. Anhydrous tetrahydrofuran, lithium hexamethyldisilazide, and phenyllithium were purchased from Sigma-Aldrich. Sodium hydrosulfite, 1,4-dioxane, and all other solvents were purchased from VWR. Phthalaldehyde was purchased from Oakwood. Quinizarin was purchased from AA Blocks and purified by passing through a silica plug with CH_2Cl_2 before use. All of the other purchased chemicals were used without further purification.

Proton and carbon NMR spectra were collected using a Bruker Avance NEO 400 MHz spectrometer. Chemical shifts of each spectrum are reported in parts per million and referenced to deuterated chloroform solvent. Mass analysis was carried out on an Agilent 6520B quadrupole-time-of-flight (Q-TOF) mass spectrometer with the manufacturer supplied atmospheric pressure chemical ionization (APCI) source installed. UV−vis absorption was performed by using a Cary 60 UV−vis spectrometer. Fluorescence spectra were collected using an Edinburgh FS5 spectrometer. Cyclic voltammetry was measured using a BAS CV-50W potentiostat at a scan rate of 50 mV/s with a glassy carbon working electrode, a platinum wire counter electrode, and a Ag/AgCl reference electrode. A solution of 0.1 M Bu_4NPF_6 in dichloromethane was used as a supporting electrolyte solution under a blanket of N_2 with F_c/F_c^+ as an internal reference. Fourier transform infrared spectroscopy was performed using a ThermoScientific Nicolet iS50 FTIR spectrometer.

9,10-Diphenyl-1,4-anthraquinone 2. Quinizarin **1** (1.0 g, 4.16 mmol) was dissolved in anhydrous THF (40 mL) under a N_2 atmosphere and cooled to 0 °C. Phenyllithium (1.9 M in dibutyl ether, 8.8 mL, 16.64 mmol) was added slowly, and the reaction mixture stirred overnight at room temperature. The reaction was quenched by addition of 10% HCl (aq) solution (40 mL) and stirred for 15 min. The product was extracted with CH_2Cl_2 (100 mL) and washed with H_2O (100 mL), and all solvent was removed by rotovap. Removal of the dibutyl ether required heating to 60 °C. The crude mixture was suspended in 3:1 CH_2Cl_2/hexanes and passed through a silica plug. Once the dark orange side products had eluted, the yellow product was eluted with CH_2Cl_2. Removal of the solvent gave quinone **2** as an orange powder (0.78 g, 52%). Single crystals suitable for X-ray diffraction were grown from slow cooling of a saturated toluene solution.

^1H NMR (400 MHz, $CDCl_3$) δ: 7.49−7.60 (10H, m), 7.27 (4H, m), 6.80 (2H, s). ^{13}C NMR (100 MHz, $CDCl_3$) 185.8, 143.6, 139.8, 139.4, 135.4, 129.0, 128.9, 128.6, 128.4, 127.3, 126.0. HRMS (APCI, + ve) m/z: $[M + H]^+$ calcd for $C_{26}H_{16}O_2$, 360.1223; found, 361.1227.

9,10-Diphenyl-1,4-anthrahydroquinone 3. 9,10-Diphenyl-1,4-anthraquinone (0.52 g, 1.44 mmol) was dissolved in 1,4-dioxane (10 mL) and H_2O (10 mL) was added. The solution was purged with N_2 gas for 30 min. Sodium hydrosulfite (1.0 g, 5.77 mmol) was added, and the reaction mixture was stirred overnight at room temperature. The product was extracted with Et_2O (100 mL) and washed with

H_2O (3 × 100 mL). The organic layer was dried over $MgSO_4$ and filtered. The solvent was removed, and the hydroquinone product **3** (a bright yellow solid with crude yield of 0.44 g) was used in the next step without further purification due to oxidative instability of hydroquinones.

Diphenyl Pentacene Quinone 4. *o*-Phthalaldehyde (0.16 g, 1.22 mmol) was added to the crude diphenyl hydroquinone **3** (0.44 g, assumed 1.22 mmol) and the flask purged with N_2. THF (10 mL) was added and then 15% KOH (aq) solution (approximately 0.5 mL) was added dropwise until a brown coloration was observed. The reaction mixture was stirred overnight at room temperature. The solvent was removed by a rotovap, and the product was triturated from methanol. After filtration, a sample of the solid was analyzed by TLC (CH_2Cl_2) and if further purification was required, the mixture was passed through a silica plug with CH_2Cl_2 and triturated from methanol once more to yield quinone **4** as a yellow microcrystalline solid (0.36 g, 55% over two steps).

Quinone **4** was not soluble enough in $CDCl_3/CS_2$ to obtain the NMR data. HRMS (APCI, + ve) *m*/*z*: $[M + H]^+$ calcd for $C_{34}H_{20}O_2$, 461.1536; found, 461.1544.

TES-PhPN. Diphenyl pentacene quinone **4** (0.300 g, 0.65 mmol) was placed in a flame-dried round-bottom flask, suspended in hexanes (40 mL) and cooled to 0 °C in an ice bath. Triethylsilyl acetylene (0.82 mL, 4.55 mmol) was added and then lithium hexamethyldisilazide (1 M in THF, 3.9 mL, 3.9 mmol) was added slowly. The reaction was stirred at room temperature for 16 h. The solvent was removed under reduced pressure and the mixture then poured onto a silica plug with hexanes. Excess acetylene was eluted with hexanes, and the pentacene diol was then eluted with 1:1 CH_2Cl_2/acetone. The solvent was removed and the diol redissolved in acetone (40 mL) and methanol (40 mL). Tin(II) chloride (0.73 g, 3.25 mmol) and 10% HCl (aq) (5 mL) were added and the reaction stirred for 1 h. The mixture was extracted with CH_2Cl_2 (100 mL) and washed with H_2O (100 mL). The product was purified by silica plug (10:1 hexanes/CH_2Cl_2). Recrystallization from 2-butanone yielded the product as dark blue rod-like crystals (0.30 g, 65%)

^1H NMR (400 MHz, $CDCl_3$) δ: 9.26 (2H, s), 7.87 (2H, dd, $J = 6.4$, 3.0 Hz), 7.50−7.57 (12H, m), 7.35 (2H, dd, $J = 6.5$, 3.2 Hz), 7.18 (2H, dd, $J = 7.0$, 3.5 Hz), 1.05 (18H, t, $J = 8.0$ Hz), 0.69 (12H, q, $J = 8.0$ Hz). ^{13}C NMR (100 MHz, $CDCl_3$) δ: 141.1, 137.4, 133.0, 132.5, 132.5, 130.9, 128.9, 128.6, 127.9, 127.9, 127.0, 126.8, 126.0, 125.6, 119.0, 114.4, 104.9, 7.8, 4.8. HRMS (APCI, + ve) *m*/*z*: $[M + H]^+$ calcd for $C_{50}H_{50}Si_2$, 707.3524; found, 707.3515.

TIPS-PhPN. Diphenyl pentacene quinone **4** (0.300 g, 0.65 mmol) was placed in a flame-dried round-bottom flask and suspended in hexanes (40 mL) and cooled to 0 °C in an ice bath. Triisopropylsilyl acetylene (1.0 mL, 4.55 mmol) was added and then lithium hexamethyldisilazide (1 M in THF, 3.9 mL, 3.9 mmol) was added slowly. The reaction was stirred at room temperature for 16 h. The solvent was removed under reduced pressure and the mixture then poured onto a silica plug with hexanes. Excess acetylene was eluted with hexanes, and the pentacene diol was then eluted with 1:1 CH_2Cl_2/acetone. The solvent was removed, and the diol was redissolved in acetone (40 mL) and methanol (40 mL). Tin(II) chloride (0.73 g, 3.25 mmol) and 10% HCl (aq) (5 mL) were added, and the reaction was stirred for 1 h. The mixture was extracted with CH_2Cl_2 and washed with H_2O. The product was purified by silica plug (10:1 hexanes/CH_2Cl_2). Recrystallization from 2-butanone yielded the product as dark blue plate-like crystals (0.34 g, 66%)

^1H NMR (400 MHz, $CDCl_3$) δ: 9.33 (2H, s), 7.86 (2H, dd, $J = 6.5$, 3.0 Hz), 7.49−7.57 (12H, m), 7.35 (2H, dd, $J = 6.8$, 3.1 Hz), 7.18 (2H, dd, $J = 6.8$, 3.4 Hz), 1.13, (42H, s). ^{13}C NMR (100 MHz, $CDCl_3$) δ: 140.8, 137.0, 133.0, 132.5, 132.5, 130.7, 128.9, 128.4, 128.1, 127.8, 126.9, 126.8, 126.0, 125.5, 119.0, 113.3, 105.9, 19.1, 12.1. HRMS (APCI, + ve) *m*/*z*: $[M + H]^+$ calcd for $C_{56}H_{62}Si_2$, 791.4463; found, 791.4460.

X-ray Crystallography. X-ray diffraction data were collected at 90.0(2) K on a Bruker D8 Venture dual-source diffractometer with graded-multilayer focused MoK(alpha) X-rays. Raw data were integrated, scaled, merged, and corrected for Lorentz-polarization effects using the APEX3 package.[27] [Bruker-AXS, 2018.] Corrections for absorption were applied using SADABS.[28] The structures were solved by dual-space methods (SHELXT)[29] and refined against F^2 by weighted full-matrix least-squares (SHELXL-2019).[30] Hydrogen atoms were found in difference maps but subsequently placed at calculated positions and refined using riding models. Non-hydrogen atoms were refined with anisotropic displacement parameters. The final structure model was checked using established methods.[31] Atomic scattering factors were taken from the International Tables for Crystallography.[32]

■ COMPUTATIONAL DETAILS

Density functional theory (DFT) calculations were performed using Gaussian 16 Rev A.03.[33] Vibrational spectra were calculated using B3LYP/6-31G* in the gas phase,[34] performing a geometry optimization followed by frequency analysis. No imaginary frequencies were observed, and the vibrational frequencies were scaled by a factor of 0.96 according to established scaling factors.[35] Theoretical IR spectra were produced by line broadening of the frequencies using GaussSum software.[36] Vibrational modes were visualized by using ChemCraft software.

Optoelectronic properties were computed by first reoptimizing the molecular geometry (ωB97XD/6-31G*,[37] where $\omega = 0.1$ Bohr^{-1} as a representative range separation parameter for conjugated polycyclic aromatics) and then optimizing the range separation factor such that Koopmans' theorem (εHOMO = −IP) was fulfilled in the gas phase.[38] The redox and optical properties (Table S6) were then recomputed using this optimized functional (IP-tuned ωB97XD/6-31G*) in the presence of a polarizable continuum mimicking chloroform solvation.

Transfer integrals were computed using the method of Valeev[39] with Gaussian 16 Rev A.03. Transfer integrals were all calculated using PBE0/6-31G* for comparison with prior calculations on similar systems, for the static atomic coordinates from the experimental crystal structure, and for coordinates extracted from the MD simulations.

Molecular Dynamics

Molecular dynamics (MD) simulations were run using GROMACS 2020 software suite[40] with the OPLS-AA force field.[41] 5 × 3 × 3 supercells were constructed using GROMACS genconf utility from the experimental X-ray single-crystal structures for TIPS-PN and TIPS-PhPN. The supercells initially energy minimized by the steepest descent algorithm[42] and equilibrated under *NVT* (constant number of molecules, volume, and temperature) and *NPT* (constant number of molecules, pressure, and temperature) ensembles. Two *NPT* simulations were done, first with Berendsen pressure coupling and second for data gathering with Parrinello−Rahman pressure coupling for 20 ns with a time step of 2 fs.[43] All equilibrium simulations were done at 77 and 293 K, respectively, employing periodic boundary conditions (PBC) in all directions. A spherical cutoff of 1.4 nm was used for both long-range (electrostatic interactions) and short-range van der Waals interactions. The particle-mesh Ewald method (PME)[44] was used to treat long-range interactions. The LINCS (LINear Constraint Solver) algorithm was employed to constrain hydrogen bonds.[45]

The force field was validated using lattice parameters from the crystallography information file (CIF) at 173 K for TIPS-PN and 100 K for TIPS-PhPN and these were compared to the MD-simulated supercell parameters for both molecules

(Tables S7 and S8). The validity of the force field for TIPS PhPN is confirmed through a simulated supercell that has a maximum deviation of less than ∼0.6%, while TIPS-PN has a deviation of less than ∼8%. The dynamic flexibility in TIPS-PN resulted in an expansion of the simulation box, which resulted in more overall volume compared to unit cell volume. In addition to that at 293 K, the expansion of simulation lattice parameters is much more visible following the same trend for TIPS-PN compared to TIPS-PhPN (Tables S9 and S10).

Symmetry Adapted Perturbation Theory (SAPT0)

SAPT0 calculations[46] were performed using Psi4 software,[47] utilizing the jun-cc-pvdz basis set[48] as reported for accurate energy values at modest computational cost.[49] Energy decomposition analysis is automatically reported in these calculation output where ES = electrostatic, EX = exchange, DISP = dispersion, and IND = induction.

Transistor Fabrication and Testing

Device Fabrication. Organic thin film transistors (OTFTs) were fabricated on Borosilicate glass similarly to previously reported procedures.[50] The glass substrates were first cleaned by sonicating in Decon 90 soap and deionized water for 10 min. This step was followed by separate 10 min sonication steps in acetone and then 10 min sonication in isopropyl alcohol (IPA), where the acetone was used to clean the Decon 90 soap off the glass substrate and the subsequent IPA then used to remove the acetone. After drying the substrates with nitrogen, they were treated with UV−ozone for 10 min. Next, 40 nm thick gold (Au) source and drain electrodes were deposited by using thermal evaporation, with an Angstrom evaporator and a shadow mask. The substrates were then immersed in a pentafluorothiophenol (PFBT)/IPA solution for 15 min, where the PFBT is used to optimize the work function of the gold electrodes to minimize contact resistance and thereby enhance charge injection into the hole transporting semiconductor layers. Excess PFBT was then removed by rinsing with IPA.

Next, the semiconductor layers were deposited in the following way: First, neat TIPS-PN and TIPS-PhPN solutions were prepared in tetralin at a concentration of 10 mg/mL. For the TIPS-PN and TIPS-PhPN thin films, 80 μL of solution was spin-coated onto the glass/electrode substrates at 500 rpm for 10 s, followed by 1000 rpm for 30 s. The films were then annealed at 90 °C for 5 min. The blend films, for both TIPS-PN or TIPS-PhPN, were prepared in tetralin at a concentration of 10 mg/mL, where the PTAA in both cases was at a 1:1 ratio with the respective small molecules. 80 μL of each blend solution was spin-coated onto the glass/electrode substrates at 500 rpm for 10 s, followed by 1000 rpm for 30 s. The TIPS-PN blend films were then annealed at 90 °C for 5 min, whereas TIPS-PhPN blend films were annealed at 60 °C for 5 min. Following deposition of the semiconductor layers, 100 μL of the dielectric, Cytop, was spin-coated at 500 rpm for 10 s and 2000 rpm for 30 s. The Cytop layer was then annealed at 50 °C for 60 min, resulting in an average thickness of 1168.34 nm. The areal capacitance of the Cytop was calculated using

$$C_{(\mathrm{areal})} = \frac{k\varepsilon_0}{d}$$

where k is the dielectric constant of Cytop (2.1), ε_0 is the permittivity of free space, and d is the thickness of the dielectric layer. Using this relation, the areal capacitance of the Cytop was determined to be 1.59×10^{-9} F/cm^2. Finally, 40 nm of Al was thermally evaporated onto the dielectric, using a shadow mask, as the gate electrode.

Device Characterization. All device characterizations were performed inside a N_2 filled glovebox using a KEYSIGHT B2912A precision source measure unit. Transfer characteristics were obtained by sweeping the gate voltage (V_G) from +5 V to −100 V, and the drain voltage (V_D) was set at −10 V for the linear regime, and −100 V for the saturation regime. Output characteristics were obtained by sweeping V_D from 0 to −100 V and fixing V_G at values from 0 V to −100 V, in 10 V increments. Data was analyzed and plotted using Origin.

Temperature-Dependent Measurements. Temperature-dependent measurements were carried out using a Lakeshore cryostation cooled with liquid nitrogen. The stage was first cooled to 77 K, and the transfer characteristics were then obtained from 77 to 300 K, in 15 °C intervals.

■ ASSOCIATED CONTENT

Data Availability Statement

The data that support the findings of this study are available from the corresponding author upon reasonable request.

Supporting Information

The Supporting Information is available free of charge at https://pubs.acs.org/doi/10.1021/acs.chemmater.6c00263.

> Characterization spectra including copies of ^{1}H and ^{13}C NMR spectra, HRMS spectra, crystallographic data, molecular dynamics simulation summary and associated density functional theory calculations, and charge mobility measurement data (PDF)

Accession Codes

Deposition numbers 2526358−2526360 contain the supplementary crystallographic data for this paper. These data can be obtained free of charge via the joint Cambridge Crystallographic Data Centre (CCDC) and Fachinformationszentrum Karlsruhe Access Structures service.

■ AUTHOR INFORMATION

Corresponding Author

Karl J. Thorley − *Center for Applied Energy Research, University of Kentucky, Lexington, Kentucky 40511, United States;* orcid.org/0000-0003-0665-3363;
Email: karl.thorley@uky.edu

Authors

Gehan S. Rupasinghe − *Center for Applied Energy Research, University of Kentucky, Lexington, Kentucky 40511, United States; Department of Chemical and Materials Engineering, University of Kentucky, Lexington, Kentucky 40506, United States*

Sashen Ruhunage − *Center for Applied Energy Research, University of Kentucky, Lexington, Kentucky 40511, United States; Department of Chemistry, University of Kentucky, Lexington, Kentucky 40506, United States;* orcid.org/0000-0002-6485-6663

Moses Ogbaje − *Center for Applied Energy Research, University of Kentucky, Lexington, Kentucky 40511, United States; Department of Chemistry, University of Kentucky, Lexington, Kentucky 40506, United States*

Vinayak Bhat − *School of Health Sciences, Columbia, South Carolina 29203, United States;* orcid.org/0000-0003-0736-3499

Sean Parkin − *Department of Chemistry, University of Kentucky, Lexington, Kentucky 40506, United States*

Chad Risko − *Center for Applied Energy Research, University of Kentucky, Lexington, Kentucky 40511, United States; Department of Chemistry, University of Kentucky, Lexington, Kentucky 40506, United States;* orcid.org/0000-0001-9838-5233

Alexandra Paterson − *Center for Applied Energy Research, University of Kentucky, Lexington, Kentucky 40511, United States; Department of Chemical and Materials Engineering, University of Kentucky, Lexington, Kentucky 40506, United States*

John E. Anthony − *Center for Applied Energy Research, University of Kentucky, Lexington, Kentucky 40511, United States; Department of Chemistry, University of Kentucky, Lexington, Kentucky 40506, United States;* orcid.org/0000-0002-8972-1888

Complete contact information is available at:
https://pubs.acs.org/10.1021/acs.chemmater.6c00263

Notes

The authors declare no competing financial interest.

ACKNOWLEDGMENTS

J.E.A. thanks NSF (DMR-2414541) for funding of synthesis and characterization. C.R. thanks NSF (DMREF-2323422) for financial support of computational analysis. The D8 Venture X-ray diffractometer was funded by the NSF (MRI CHE1625732) and by the University of Kentucky. G.S.R. and A.F.P. thank the Defense Advanced Research Projects Agency (DARPA) for financial support through grant number D24AP00298-01 and National Science Foundation (NSF) through grant number 2441261.

REFERENCES

(1) Anthony, J. E.; Brooks, J. S.; Eaton, D. L.; Parkin, S. R. Functionalized Pentacene: Improved Electronic Properties from Control of Solid-State Order. *J. Am. Chem. Soc.* **2001**, *123* (38), 9482−9483.

(2) Anthony, J. E.; Eaton, D. L.; Parkin, S. R. A Road Map to Stable, Soluble, Easily Crystallized Pentacene Derivatives. *Org. Lett.* **2002**, *4* (1), 15−18.

(3) Fratini, S.; Ciuchi, S.; Mayou, D.; de Laissardière, G. T.; Troisi, A. A map of high-mobility molecular semiconductors. *Nat. Mater.* **2017**, *16* (10), 998−1002.

(4) Troisi, A.; Orlandi, G.; Anthony, J. E. Electronic Interactions and Thermal Disorder in Molecular Crystals Containing Cofacial Pentacene Units. *Chem. Mater.* **2005**, *17* (20), 5024−5031.

(5) Nematiaram, T.; Troisi, A. Strategies to reduce the dynamic disorder in molecular semiconductors. *Mater. Horiz.* **2020**, *7* (11), 2922−2928.

(6) (a) Brédas, J. L.; Calbert, J. P.; da Silva Filho, D. A.; Cornil, J. Organic Semiconductors: A Theoretical Characterization of the Basic Parameters Governing Charge Transport. *Proc. Natl. Acad. Sci. U. S. A.* **2002**, *99* (9), 5804−5809. (b) Coropceanu, V.; Cornil, J.; da Silva Filho, D. A.; Olivier, Y.; Silbey, R.; Brédas, J.-L. Charge Transport in Organic Semiconductors. *Chem. Rev.* **2007**, *107* (4), 926−952.

(7) (a) Eggeman, A. S.; Illig, S.; Troisi, A.; Sirringhaus, H.; Midgley, P. A. Measurement of molecular motion in organic semiconductors by thermal diffuse electron scattering. *Nat. Mater.* **2013**, *12* (11), 1045−1049. (b) Illig, S.; Eggeman, A. S.; Troisi, A.; Jiang, L.; Warwick, C.; Nikolka, M.; Schweicher, G.; Yeates, S. G.; Henri Geerts, Y.; Anthony, J. E.; Sirringhaus, H. Reducing dynamic disorder in small-molecule organic semiconductors by suppressing large-amplitude thermal motions. *Nature Commun.* **2016**, *7*, 10736.

(8) Payne, M. M.; Delcamp, J. H.; Parkin, S. R.; Anthony, J. E. Robust, Soluble Pentacene Ethers. *Org. Lett.* **2004**, *6* (10), 1609−1612.

(9) Wasikiewicz, J. M.; Abu-Sen, L.; Horn, A. B.; Koelewijn, J. M.; Parry, A. V. S.; Morrison, J. J.; Yeates, S. G. Towards solution processable air stable p-type organic semiconductors: synthesis and evaluation of mono and di-fluorinated pentacene derivatives. *J. Mater. Chem. C* **2016**, *4*, 7309−7315.

(10) Llorente, G. R.; Dufourg-Madec, M.-B.; Crouch, D. J.; Pritchard, R. G.; Ogier, S.; Yeates, S. G. High performance, acene-based organic thin film transistors. *Chem. Commun.* **2009**, 3059−3061.

(11) Zhang, J.; Sarrafpour, S.; Haas, T. E.; Müller, P.; Thomas, S. W. Structure, photophysics, and photooxidation of crowded diethynyltetracenes. *J. Mater. Chem.* **2012**, *22* (13), 6182.

(12) Paraskar, A. S.; Reddy, A. R.; Patra, A.; Wijsboom, Y. H.; Gidron, O.; Shimon, L. J. W.; Leitus, G.; Bendikov, M. Rubrenes: Planar and Twisted. *Chem.—Eur. J.* **2008**, *14* (34), 10639−10647.

(13) McGarry, K. A.; Xie, W.; Sutton, C.; Risko, C.; Wu, Y.; Young, V. G.; Brédas, J.-L.; Frisbie, C. D.; Douglas, C. J. Rubrene-Based Single-Crystal Organic Semiconductors: Synthesis, Electronic Structure, and Charge-Transport Properties. *Chem. Mater.* **2013**, *25* (11), 2254−2263.

(14) Sutton, C.; Marshall, M. S.; Sherrill, C. D.; Risko, C.; Brédas, J.-L. Rubrene The Interplay between Intramolecular and Intermolecular Interactions Determines the Planarization of Its Tetracene Core in the Solid State. *J. Am. Chem. Soc.* **2015**, *137* (27), 8775−8782.

(15) Ogden, W. A.; Ghosh, S.; Bruzek, M. J.; Mcgarry, K. A.; Balhorn, L.; Young, V.; Purvis, L. J.; Wegwerth, S. E.; Zhang, Z.; Serratore, N. A.; Cramer, C. J.; Gagliardi, L.; Douglas, C. J. Partial Fluorination as a Strategy for Crystal Engineering of Rubrene Derivatives. *Cryst. Growth Des.* **2017**, *17* (2), 643−658.

(16) Lu, J.; Ho, D. M.; Vogelaar, N. J.; Kraml, C. M.; Pascal, R. A. A pentacene with a 144° twist. *J. Am. Chem. Soc.* **2004**, *126* (36), 11168−11169.

(17) Norton, J. E.; Houk, K. N. Electronic structures and properties of twisted polyacenes. *J. Am. Chem. Soc.* **2005**, *127* (12), 4162−4163.

(18) Freudenberg, J.; Bunz, U. H. F. How to Stabilize Large Soluble (Hetero-)Acenes. *J. Am. Chem. Soc.* **2024**, *146* (25), 16937−16949.

(19) Scott, A. P.; Radom, L. Harmonic vibrational frequencies: An evaluation of Hartree-Fock, Møller-Plesset, quadratic configuration interaction, density functional theory, and semiempirical scale factors. *J. Phys. Chem.* **1996**, *100* (41), 16502−16513.

(20) Adamo, C.; Barone, V. Toward reliable density functional methods without adjustable parameters: The PBE0 model. *J. Chem. Phys.* **1999**, *110* (13), 6158.

(21) Sutton, C.; Sears, J. S.; Coropceanu, V.; Brédas, J.-L. Understanding the Density Functional Dependence of DFT-Calculated Electronic Couplings in Organic Semiconductors. *J. Phys. Chem. Lett.* **2013**, *4* (6), 919−924.

(22) Thorley, K. J.; Finn, T. W.; Jarolimek, K.; Anthony, J. E.; Risko, C. Theory-Driven Insight into the Crystal Packing of Trialkylsilylethynyl Pentacenes. *Chem. Mater.* **2017**, *29* (6), 2502−2512.

(23) Parker, T. M.; Burns, L. A.; Parrish, R. M.; Ryno, A. G.; Sherrill, C. D. Levels of symmetry adapted perturbation theory (SAPT). I. Efficiency and performance for interaction energies. *J. Chem. Phys.* **2014**, *140* (9), 094106.

(24) Hehre, W. J.; Ditchfield, R.; Pople, J. A. Self-Consistent Molecular Orbital Methods. XII. Further Extensions of Gaussian-Type Basis Sets for Use in Molecular Orbital Studies of Organic Molecules. *J. Chem. Phys.* **1972**, *56* (5), 2257−2261.

(25) (a) Losi, T.; Viola, F. A.; Sala, E.; Heeney, M.; He, Q.; Kleemann, H.; Caironi, M. Downscaling of Organic Field-Effect Transistors based on High-Mobility Semiconducting Blends for High-Frequency Operation. *Small Methods* **2024**, *8* (12), 2400546. (b) Paterson, A. F.; Treat, N. D.; Zhang, W.; Fei, Z.; Wyatt-Moon, G.; Faber, H.; Vourlias, G.; Patsalas, P. A.; Solomeshch, O.; Tessler, N.; Heeney, M.; Anthopoulos, T. D. Small Molecule/Polymer Blend Organic Transistors with Hole Mobility Exceeding 13 cm2 V−1 s−1.

Adv. Mater. **2016**, *28* (35), 7791−7798. (c) Smith, J.; Zhang, W.; Sougrat, R.; Zhao, K.; Li, R.; Cha, D.; Amassian, A.; Heeney, M.; McCulloch, I.; Anthopoulos, T. D. Solution-Processed Small Molecule-Polymer Blend Organic Thin-Film Transistors with Hole Mobility Greater than 5 cm2/Vs. *Adv. Mater.* **2012**, *24* (18), 2441−2446. (d) Hamilton, R.; Smith, J.; Ogier, S.; Heeney, M.; Anthony, J. E.; McCulloch, I.; Veres, J.; Bradley, D. D. C.; Anthopoulos, T. D. High-Performance Polymer-Small Molecule Blend Organic Transistors. *Adv. Mater.* **2009**, *21* (10−11), 1166−1171.

(26) Sakanoue, T.; Sirringhaus, H. Band-like temperature dependence of mobility in a solution-processed organic semiconductor. *Nat. Mater.* **2010**, *9* (9), 736−740.

(27) *Bruker-AXS APEX2/3*, 2018.

(28) Krause, L.; Herbst-Irmer, R.; Sheldrick, G. M.; Stalke, D. Comparison of silver and molybdenum microfocus X-ray sources for single-crystal structure determination. *J. Appl. Crystallogr.* **2015**, *48* (1), 3−10.

(29) Sheldrick, G. M. SHELXT − Integrated space-group and crystal-structure determination. *Acta Crystallogr. A Found. Adv.* **2015**, *71* (1), 3−8.

(30) Sheldrick, G. M. Crystal structure refinement with SHELXL. *Acta Crystallogr., Sect. C:Struct. Chem.* **2015**, *71* (1), 3−8.

(31) (a) Parkin, S. Expansion of scalar validation criteria to three dimensions: the R tensor. *Acta Crystallogr., Sect. A:Found. Crystallogr.* **2000**, *56* (2), 157−162. (b) Spek, A. L. checkCIF validation ALERTS: what they mean and how to respond. *Acta Crystallogr., Sect. E:Crystallogr. Commun.* **2020**, *76* (1), 1−11.

(32) Wilson, A. J. C. *International Tables for Crystallography, Vol C: Mathematical, Physical and Chemical Tables*; Kluwer Academic Publishers, 1992.

(33) *Gaussian 16* Rev. A.03; Gaussian: Wallingford, CT, 2016.

(34) (a) Hariharan, P. C.; Pople, J. A. The influence of polarization functions on molecular orbital hydrogenation energies. *Theor. Chim. Acta* **1973**, *28* (3), 213−222. (b) Hehre, W. J.; Ditchfield, R.; Pople, J. A. Self-Consistent Molecular Orbital Methods. XII. Further Extensions of Gaussian-Type Basis Sets for Use in Molecular Orbital Studies of Organic Molecules. *J. Chem. Phys.* **1972**, *56* (5), 2257−2261. (c) Becke, A. D. Density-functional thermochemistry. III. The role of exact exchange. *J. Chem. Phys.* **1993**, *98* (7), 5648−5652.

(35) Scott, A. P.; Radom, L. Harmonic Vibrational Frequencies: An Evaluation of Hartree−Fock, Møller−Plesset, Quadratic Configuration Interaction, Density Functional Theory, and Semiempirical Scale Factors. *J. Phys. Chem.* **1996**, *100* (41), 16502−16513.

(36) O'Boyle, N. M.; Tenderholt, A. L.; Langner, K. M. cclib: A library for package-independent computational chemistry algorithms. *J. Comput. Chem.* **2008**, *29*, 839−845.

(37) Chai, J.-D.; Head-Gordon, M. Long-range corrected hybrid density functionals with damped atom−atom dispersion corrections. *Phys. Chem. Chem. Phys.* **2008**, *10*, 6615−6620.

(38) Moser, M.; Thorley, K. J.; Moruzzi, F.; Ponder, J. F.; Maria, I. P.; Giovannitti, A.; Inal, S.; McCulloch, I. Highly selective chromoionophores for ratiometric Na+ sensing based on an oligoethyleneglycol bridged bithiophene detection unit. *J. Mater. Chem. C* **2019**, *7* (18), 5359−5365.

(39) Valeev, E. F.; Coropceanu, V.; da Silva Filho, D. A.; Salman, S.; Brédas, J.-L. Effect of Electronic Polarization on Charge-Transport Parameters in Molecular Organic Semiconductors. *J. Am. Chem. Soc.* **2006**, *128* (30), 9882−9886.

(40) Van Der Spoel, D.; Lindahl, E.; Hess, B.; Groenhof, G.; Mark, A. E.; Berendsen, H. J. GROMACS: fast, flexible, and free. *J. Comput. Chem.* **2005**, *26* (16), 1701−1718.

(41) (a) Jorgensen, W. L.; Maxwell, D. S.; Tirado-Rives, J. Development and Testing of the OPLS All-Atom Force Field on Conformational Energetics and Properties of Organic Liquids. *J. Am. Chem. Soc.* **1996**, *118* (45), 11225−11236. (b) Dodda, L. S.; Cabeza de Vaca, I.; Tirado-Rives, J.; Jorgensen, W. L. LigParGen web server: an automatic OPLS-AA parameter generator for organic ligands. *Nucleic Acids Res.* **2017**, *45* (W1), W331−W336.

(42) Wardi, Y. A stochastic steepest-descent algorithm. *J. Optim. Theor. Appl.* **1988**, *59* (2), 307−323.

(43) (a) Berendsen, H. J. C.; Postma, J. P. M.; van Gunsteren, W. F.; DiNola, A.; Haak, J. R. Molecular dynamics with coupling to an external bath. *J. Chem. Phys.* **1984**, *81* (8), 3684−3690. (b) Parrinello, M.; Rahman, A. Polymorphic transitions in single crystals: A new molecular dynamics method. *J. Appl. Phys.* **1981**, *52* (12), 7182−7190.

(44) Darden, T.; York, D.; Pedersen, L. Particle mesh Ewald: An N·log(N) method for Ewald sums in large systems. *J. Chem. Phys.* **1993**, *98* (12), 10089−10092.

(45) Hess, B.; Bekker, H.; Berendsen, H. J. C.; Fraaije, J. G. E. M. LINCS: A linear constraint solver for molecular simulations. *J. Comput. Chem.* **1997**, *18* (12), 1463−1472.

(46) (a) Hohenstein, E. G.; Parrish, R. M.; Sherrill, C. D.; Turney, J. M.; Schaefer, H. F., III Large-scale symmetry-adapted perturbation theory computations via density fitting and Laplace transformation techniques: Investigating the fundamental forces of DNA-intercalator interactions. *J. Chem. Phys.* **2011**, *135* (17), 174107. (b) Hohenstein, E. G.; Sherrill, C. D. Density fitting and Cholesky decomposition approximations in symmetry-adapted perturbation theory: Implementation and application to probe the nature of π-π interactions in linear acenes. *J. Chem. Phys.* **2010**, *132* (18), 184111.

(47) Smith, D. G. A.; Burns, L. A.; Simmonett, A. C.; Parrish, R. M.; Schieber, M. C.; Galvelis, R.; Kraus, P.; Kruse, H.; Di Remigio, R.; Alenaizan, A.; et al. PSI4 1.4: Open-source software for high-throughput quantum chemistry. *J. Chem. Phys.* **2020**, *152* (18), 184108.

(48) Papajak, E.; Truhlar, D. G. Convergent Partially Augmented Basis Sets for Post-Hartree−Fock Calculations of Molecular Properties and Reaction Barrier Heights. *J. Chem. Theor. Comput.* **2011**, *7* (1), 10−18.

(49) Parker, T. M.; Burns, L. A.; Parrish, R. M.; Ryno, A. G.; Sherrill, C. D. Levels of symmetry adapted perturbation theory (SAPT). I. Efficiency and performance for interaction energies. *J. Chem. Phys.* **2014**, *140* (9), 094106.

(50) (a) Hunter, S.; Chen, J.; Anthopoulos, T. D. Microstructural Control of Charge Transport in Organic Blend Thin-Film Transistors. *Adv. Funct. Mater.* **2014**, *24*, 5969−5976. (b) Hunter, S.; Anthopoulos, T. D. Observation of Unusual, Highly Conductive Grain Boundaries in High-Mobility Phase Separated Organic Semiconducting Blend Films Probed by Lateral-Transport Conductive-AFM. *Adv. Mater.* **2013**, *25*, 4320−4326. (c) Paterson, A. F.; Treat, N. D.; Zhang, W.; Fei, Z.; Wyatt-Moon, G.; Faber, H.; Vourlias, G.; Patsalas, P. A.; Solomeshch, O.; Tessler, N.; Heeney, M.; Anthopoulos, T. D. Small Molecule/Polymer Blend Organic Transistors with Hole Mobility Exceeding 13 cm^2 V^{-1} s^{-1}. *Adv. Mater.* **2016**, *28*, 7791−7798. (d) Hunter, S.; Mottram, A. D.; Anthopoulos, T. D. Temperature and composition-dependent density of states in organic small-molecule/polymer blend transistors. *J. Appl. Phys.* **2016**, *120*, 025502. (e) Smith, J.; Heeney, M.; McCulloch, I.; Nekuda Malik, J.; Stingelin, N.; Bradley, D. D. C.; Anthopoulos, T. D. Percolation behaviour in high mobility p-channel polymer/small-molecule blend organic field-effect transistors. *Org. Electron.* **2011**, *12*, 143−147.